

The Stray Loss on Magnetic Shielding in Power Transformers

SUMEI YANG¹, ZHIGUANG CHENG², QINGXIN YANG¹, XIAOQUAN ZHU¹

¹ Province-Ministry Joint Key Laboratory of Electromagnetic Field and Electrical Apparatus Reliability

Hebei University of Technology

Hebei University of Technology

Guangrongdao str.8 Tianjin, 300130

CHINA

² R & D Center

Baoding Tianwei Group

Baoding Tianwei Group Baoding, 071056

CHINA

Abstract: -This paper details the electromagnetic behavior and the effects of magnetic and electromagnetic shields used in large power transformers based on engineering-oriented benchmark models, and presents some newly calculated and measured results both the magnetic field and stray-field loss related to the models, and examine the engineering applicability of 3-D eddy current analysis methods and the practical loss modeling.

Key-Words: - anisotropy, hysteresis, lamination, magnetic shielding, stray loss.

1 Introduction

In the large power transformers the stray-field loss and the local loss density caused in the conducting parts are considerably increased with the capacity, which probably result in the hazardous local overheating and/or cause the insulation material destroyed, consequently endanger the transformer running.

In the electromagnetic design of larger power transformer, the stray-field loss must be controlled in an acceptable level for saving energy, as well as avoiding the un-allowed overheating. So the possible engineering strategies to cope with it have been adopted, such as the optimum material configuration and structures, and any possible shielding, etc. An example of the magnetic shields installed inside the oil-tank of a large power transformer is shown in Fig.1, which is the industrial background of the following proposal.

The paper aims to quantitatively investigate the effects of both the magnetic and electromagnetic on reducing power loss in the conducting parts through two sets of engineering-oriented benchmark shielding models named Problem 21^c, which have been built up by the authors (see the definition of the benchmark models at www.compumag.co.uk/TEAM, validate the applicability of the CEM-based analysis

methods, and provide some helpful guidance to design the shielding structures.

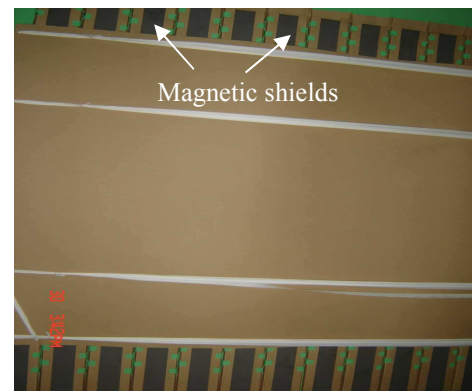


Fig.1. Magnetic shields installed in power transformer

2 Description of the Model

The electromagnetic shielding is used to prevent the leakage magnetic flux into the conducting parts by the reaction of the eddy current field induced in the shields of high conductivity, which is also called electromagnetic screen; however the magnetic shielding makes the leakage magnetic flux changing the path into the shields of high permeability, named magnetic shunt.

Problem 21^c includes magnetic (M) and electromagnetic (EM) shields[6], making of the anisotropic silicon steel sheets and the copper plates respectively. The shields are of two types, either having one single silicon steel sheet or copper plate, referred to as type 1(i.e., models P21^c-M1 or P21^c-EM1), or three separated ones, referred to as type 2(i.e., models P21^c-M2 or P21^c-EM2). The dimensions of the corresponding magnetic and electromagnetic shields are the same as shown in Figs.2~3.

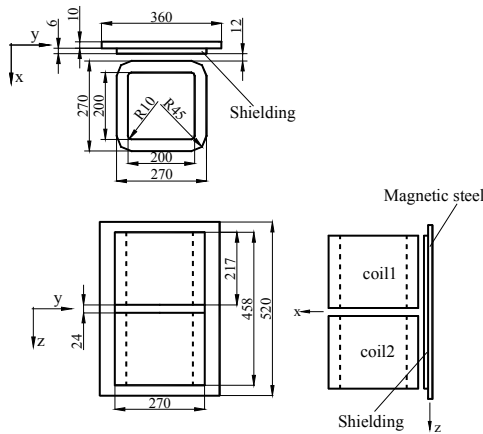


Fig. 2. Shielding model (Type 1).

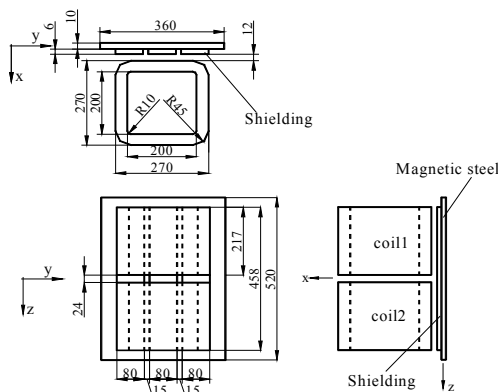


Fig.3. Shielding model (Type 2).

The design data of the shielding models involve two parts, i.e., the exciting source used in every model, and the different kinds of conducting parts driven by the exciting coils and used in different sub-models. The detailed parameters are as following:

A Exciting Source

There are two exciting coils with the same dimension, in which the exciting currents flowing in two coils are in opposite directions. The number of turns of each coil: 300; the exciting currents: ±10A (50Hz, rms).

B Conductor

1)Magnetic steel plate (A3, used in P21-B/P21^c)

The thickness of the plate: 10mm;
 the conductivity: $\sigma=6.484 \times 10^6$ S/m;
 the assumed density: 7.8×10^3 kg/m³.
 The B-H and Wh-Bm curves of magnetic steel can be found in [2].

2)Copper plate (used in P21^c-EM)

The dimension: 458×270×6 mm (in P21^c-EM1) and 458×80×6 mm (in P21^c-EM2);
 the conductivity: $\sigma=5.7143 \times 10^7$ S/m;
 the assumed density: 8.9×10^3 kg/m³;
 the relative permeability is equal to 1.

1) 3) silicon steel sheet (30RGH120, used in P21^c-M)

Laminations thickness: 6mm;

The dimension:

458×270×6mm(in P21^c-M1)and

458×80×6 mm (in P21^c-M2);

The conductivity: $\sigma=2.22 \times 10^6$ S/m;

The assumed density: 7.65×10^3 kg/m³.

The B-H, Wh-Bm and W-Bm curves are measured only in the rolling direction (z-axis) and the transverse direction (y-axis) of the sheets [2].

3 Problem Formulation

The authors have developed the eddy current codes based on different potential sets, for example, Ar-V-Ar code (Ar, the reduced magnetic vector potential, the total magnetic vector potential $A = A_r + A_s$, A_s represented the contribution of the source) is used in the paper. The non-linearity of the magnetic materials and the anisotropy of the silicon steel sheets (30RGH120) are taken into account in shield modeling.

The equations in both conducting and non-conducting regions are as follows:

In conducting regions,

$$\left. \begin{aligned} \nabla \times \frac{1}{\mu} \nabla \times (A_r + A_s) - \nabla \left(\frac{1}{\mu_c} \nabla \cdot A_r \right) + \sigma \left(\frac{\partial A_r}{\partial t} + \frac{\partial A_s}{\partial t} + \nabla V \right) &= 0 \\ \nabla \cdot \sigma \left(-\frac{\partial A_r}{\partial t} - \frac{\partial A_s}{\partial t} - \nabla V \right) &= 0 \end{aligned} \right\} (1)$$

In non-conducting regions,

$$\nabla \times \frac{1}{\mu_0} \nabla \times (A_r + A_s) - \nabla \left(\frac{1}{\mu_0} \nabla \cdot A_r \right) = J_s (2)$$

Where, the Coulomb gauging condition has been imposed. $\nabla \left(\frac{1}{\mu_c} \nabla \cdot A_r \right)$ and $\nabla \left(\frac{1}{\mu_0} \nabla \cdot A_r \right)$ are the penalty function terms to enforce the zero divergence

condition for the nodal code, in which the ‘isotropic’ permeability μ_c ensures the symmetry of finite element matrix[3]. In this paper, μ_c is chosen as the average value of μ_r of one local node in different directions.

$$\mu_{c(ne)} = (\mu_{x(ne)} + \mu_{y(ne)} + \mu_{z(ne)}) / 3 \quad (3)$$

Note that the determination of the far field boundary conditions and the symmetry conditions should be considered to fix the tangential or the normal components of the total magnetic vector potential $A = Ar + As$ there, but not Ar only.

The treatments of time differential terms have been implemented by using both time-stepping and time-harmonic methods. The non-linearity of magnetic materials has been dealt with the quasi-nonlinear scheme[3].

4 Problem Solution

4.1 Material Modeling of the Silicon Steel Lamination

To deal with the anisotropy of the silicon steel lamination used in P21°-M models, the anisotropic B-H and Wh-Bm curves have been measured in both rolling and transverse directions[2], by EPLAB of Okayama University, Japan.

In the magnetic shielding models of P21°-M, the thickness of the silicon steel sheet is only 0.3mm. It is difficult to make very thin mesh-layers in 3-D eddy current finite element analysis of a large size model. Meanwhile, the characteristics of the single silicon steel sheet are different from those of the laminated silicon shields. Thus a effective method is that silicon lamination should be regarded as virtual solid material and the effective permeability [6] is adopted in material modeling of silicon lamination. According the continuity of B and H at the interface between air and silicon steel, the effective permeability both in the plane of the lamination (tangential to the lamination) and in the normal direction is given by the following two formulas respectively:

$$\mu_t = \frac{B_t}{H_t} = \frac{\left[f \frac{\mu_{steel}}{\mu_0} + (1-f) \right] B_{air}}{\frac{B_{air}}{\mu_0}} = f \mu_{steel} + (1-f) \mu_0 \quad (4)$$

$$\mu_n = \frac{\mu_{steel} \mu_0}{f \mu_0 + (1-f) \mu_{steel}} \quad (5)$$

Where, f is the packing factor of the silicon steel lamination.

Since $\mu_{steel} \gg \mu_0$, the final effective permeability can be taken by the followings:

$$\mu_t = f \mu_{steel} \quad (6)$$

$$\mu_n = \frac{\mu_0}{(1-f)} \quad (7)$$

We can choose the effective permeability of the silicon lamination in X, Y and Z directions as follows:

$$\mu_x = \frac{\mu_0}{(1-f)} \quad (8)$$

$$\mu_y = f \mu_{ysteel} \quad (9)$$

$$\mu_z = f \mu_{zsteel} \quad (10)$$

4.2 Hysteresis Loss Calculation

A practical way to solve the engineering hysteresis loss problem has been proposed by the authors[5], i.e., the hysteresis loss (Wh) is treated to be as a function of the peak value of the flux density (Bm), and the Wh-Bm curve can be measured in advance for a specified material, as well as the B-H curve, according the following relationship.

$$W_h = \sum_{e=1}^{Ne} W_h^{(e)}(B_m^{(e)}) \rho V^{(e)} \quad (11)$$

Where, $W_h^{(e)}$ - hysteresis loss of element (W/kg).

$B_m^{(e)}$ - the peak value of the flux density.

ρ - the density of silicon.

$V^{(e)}$ - volume of element.

Ne - total number of element.

5 Experiment

The magnetic flux densities at the specified positions for P21° models have been measured using the Gauss Meter, 9200, F.W.Bell, Inc. The total losses generated in the magnetic steel plate, shields and coils have been measured using the Wide Band Power Analyzer, (D6100, LEM Instrument & Meters Co., LTD). see[3] for further detail.

6 New results

Some newly calculated and measured results of both the magnetic fields at the specified positions in air and the stray loss generated in shielding configuration have been obtained by the authors.

6.1 magnetic Flux density distribution

For magnetic Flux density distribution as Part of the results, the distributions of Bx at specified

position of the model P21^c-M2 are shown in Figs.4-5, It can be seen that the measured and calculated results practically agree well,so the effectiveness of the electromagnetic analysis methods have been proved.

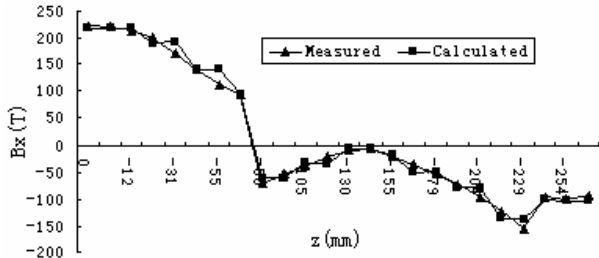


Fig.4. Bx distribution at x=3.76mm,y=0.0mm

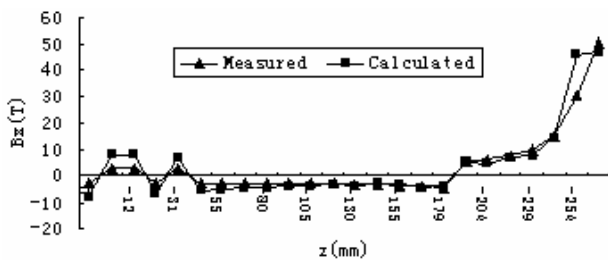


Fig.5. Bx distribution at x=-13.76mm,y=0.0mm

6.2 Stray-Field Loss Analysis

In large power transformer, the stray-loss problem is highly concerned in electromagnetic design. The two types of benchmark shielding models is closely related to the actual practice, so that the calculated and measured results of the stray loss in P21^c-EM/M models have more engineering significance to optimize design for large power transformer. The calculated loss results are shown in Table 1. To compare the shielding models with P21-B, the result of model P21-B is included in Table 1. The comparison between the calculated and measured loss results is shown in Fig.6.

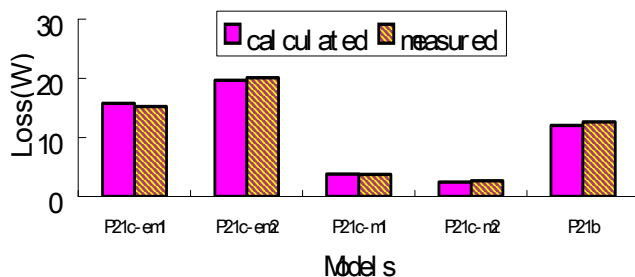
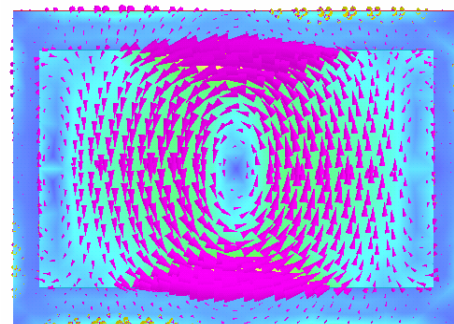


Fig.6. The calculated and measured loss results.

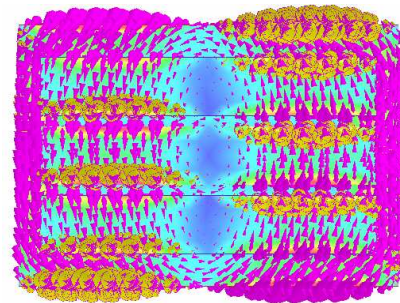
Table 1
Stray Losses Caused in Parts of P21^c and P21-B

Models	Magnetic plate	Shields	Eddy current	Hysteresis
P21-B	12.31	---	8.22	4.09
P21 ^c -EM1	5.05	10.76	14.41	1.40
P21 ^c -EM2	10.47	9.18	17.24	2.41
P21 ^c -M1	1.20	2.59	3.08	0.71
P21 ^c -M2	2.10	0.37	1.71	0.75

The eddy current distributions induced in the magnetic and electromagnetic shielding models are distinctly different, which result in the different loss distribution. Fig.7 shows the eddy current distributions of P21^c-EM1 and P21^c-M2 models, obtained by using ELEKTRA, Vector Fields, UK.



(a) P21^c-EM1 model



(b) P21^c-M2 model

Fig.7. Eddy current distributions.

It can be seen that the calculated and measured loss results practically agree well, which can be summarized as follows:

- 1) The values of total stray-field losses of the P21^c shielding models are not always less than that of P21-B without shielding. In some case the total loss generated in whole shielding structures may be increased comparing with P21-B model.
- 2) In P21^c-EM1 model, the shield is made of a single copper plate, in which the stronger eddy currents are induced to prevent the leakage magnetic flux into magnetic plate. Unfortunately the larger eddy current loss is produced there.

3) The further examination shows that the shielding effect of P21^c-EM1 is better than that of P21^c-EM2, so that the total loss of P21^c-EM2 is greater than that of P21^c-EM1. This implies that the shielding effect of the separated copper plate of P21^c-EM2 is lower than that of one-piece plate of P21^c-EM1. The main reason is that the quantity of leakage magnetic flux entering into the magnetic steel plate in the case of P21^c-EM2 is more than that of P21^c-EM1, thereby much more eddy current is induced there.

4) In P21^c-M model, the shielding parts consist of silicon steel laminations with high permeability, which absorb most leakage magnetic flux into itself, but not into magnetic plate to form a shut path. The eddy current loss produced in the thin silicon steel sheet is usually negligible. The total loss of the P21^c-M models will be remarkably reduced.

5) The total stray-field loss in P21^c-M1 is greater than that in P21^c-M2. The reason may be that, (a) the permeability of the silicon steel (30RGH120) is much higher than that of the magnetic steel(A3), therefore the leakage magnetic flux enter into the silicon steel sheets but not into the magnetic plate, this is true for both P21^c-M1 and P21^c-M2; (b) the total volume of the P21^c-M1 is larger than that of P21^c-M2; (c) the eddy current loss caused in P21^c-M1 is much greater than that of P21^c-M2. It is also shown that is the essential portion of the total loss in P21^c-M1.

6) The comparisons between the loss results of the every shielding models suggest that the effects of the magnetic shunt on reducing loss is better than that of the electromagnetic screen. However this does not mean that the electromagnetic shielding can not be used elsewhere for other purpose.

7) The eddy currents caused in the laminated sheets almost two dimensionally, which do not pass through from one sheet to another. Then only two components of total power losses in the rolling and transverse directions in the grain-oriented silicon lamination sheets are considered.

For further investigation the shielding effects and the stray-field loss of P21^c models, some extensively numerical analysis and measurement have been carried out, the test results are shown in Figs.8~9.

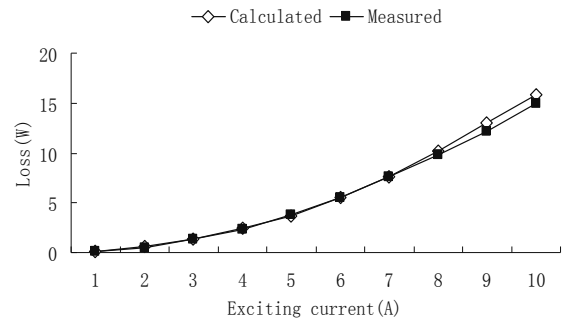


Fig.8. Loss variation with exciting currents in P21^c-EM1.

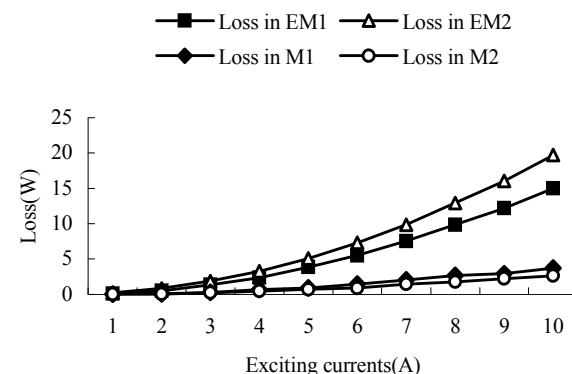


Fig.9. Loss varying with exciting currents in P21^c (Measured).

Fig.8 shows that the calculated and measured results agree well in P21^c-EM1, so it proves that the approaches of the calculation and measurement are correct, and the results can be approved. From Fig.9, it can be seen that loss varying with exciting currents in P21^c benchmark models.

5 Conclusions

The 3-D nonlinear and anisotropy eddy current hysteresis analysis and validation of the shielding benchmark models have been developed, the calculated and measured results agree well.

- 1) The Ar-V-Ar analysis method is advisable for the shielding models.
- 2) The shielding effects of P21^c benchmark models have been compared with each other. This will help the electromagnetic optimizing design in large power transformers.
- 3) Practical approaches have been provided for dealing with the non-linearity, the anisotropy and the silicon steel lamination sheet structure.
- 4) Some extended validation of the electromagnetic analysis methods have been done to further investigate the effects of exciting condition on the stray-field loss.

References

- [1] Z.Cheng, Q.Hu, S.Gao, Z.Liu, C.Ye, M.Wu, J.Wang and H.Zhu, "An engineering-oriented loss model (Problem 21)," Proc. of the international TEAM Workshop, Miami, 1993, pp.137-143(see updated TEAM Problem 21 at www.compumag.co.uk-TEAM)
- [2] Z.Cheng, N.Takahashi, S.Yang, T.Asano, Q.Hu and X.Ren, "Proposal of Problem 21-based shielding model (Problem 21'," Proc. of TEAM Workshop, Shenyang, 2005.
- [3] Z.Cheng, S.Gao and L.Li, Eddy Current Analysis and Validation in Electrical Engineering, Higher Education Press, Beijing, 2001.
- [4] Z.Cheng, R.Hao, N.Takahashi, Q.Hu and C.Fan, "Engineering-oriented benchmarking of Problem 21 family and experimental verification,"IEEE Trans.on Magn.,vol. 40, no.2, 2004,pp.1394-1397
- [5] N.Takahashi, T.Sakura and Z.Cheng, "Nonlinear analysis of eddy current and hysteresis losses of 3-D stray field loss model (Problem 21)," IEEE Trans. on Magn.,vol.37,no.5,2001,pp.3672-3675.
- [6] User Guides and Reference Manuals, OPERA V10.5, Vector Fields, UK.pp.3672-3675.